The variation of surface free energy of Al during superhydrophobicity processing

Toktam Rezayi [a], Mohammad H. Entezari [a,b,c,*], Fatemeh Moosavi [c,*]

[a] Sonochemical Research Center, Department of Chemistry, Ferdowsi University of Mashhad, 9177948974 Mashhad, Iran
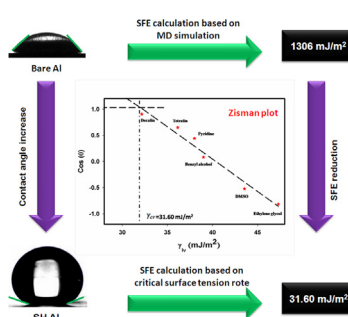[b] Environmental Chemistry Research Center, Department of Chemistry, Ferdowsi University of Mashhad, 9177948974 Mashhad, Iran
[c] Department of Chemistry, Ferdowsi University of Mashhad, 9177948974 Mashhad, Iran

HIGHLIGHTS

- Surface free energy variation after superhydrophobicity creation of Al surface is examined.
- Molecular dynamics simulation is employed for surface free energy calculation of bare Al.
- For superhydrophobic Al, critical surface tension approach was used to measure surface free energy.
- Both experimental and theoretical approaches verify surface free energy reduction after superhydrophobicity creation.

GRAPHICAL ABSTRACT

ARTICLE INFO

ABSTRACT

Surface free energy (SFE) of solids is a main property. This parameter can be affected by various phenomena such as superhydrophobicity creation. Two circumstances are necessary to achieve superhydrophobicity characteristics. These requirements are roughness improvement as well as surface energy reduction. The ZnO nanoparticle deposition is a suitable method for obtaining desirable roughness and consequently decreased SFE with stearic acid (STA) ethanol solution. The SFE of bare Al at room temperature was investigated using molecular dynamics (MD) simulation. After fabrication of superhydrophobicity property on Al surface, its SFE was calculated by applying equation of state and critical surface tension methods. The comparison between results based on two considered methods led to the fact that SFE significantly reduces after superhydrophobicity processing and reaches to STA, applied as a modifier, surface tension value. In addition to the theoretical results, water contact angle (CA) measurements confirm the SFE reduction due to superhydrophobic processing. Furthermore, the presence of STA on the superhydrophobic surface can be verified experimentally with Fourier transform infrared in conjunction with attenuated total reflection (FTIR-ATR) analysis. Therefore, both computational and experimental results approve the existence of STA on superhydrophobic Al surface and its grafting may lead to SFE reduction.

© 2017 Elsevier B.V. All rights reserved.

1. Introduction

It is believed that solid surface free energy (SFE) is a major property, which can control various phenomena, such as, the rate of sintering and the stress for brittle fracture [1]. One of the well-known

* Corresponding authors at: Sonochemical Research Center, Department of Chemistry, Ferdowsi University of Mashhad, 9177948974 Mashhad, Iran (M.H. Entezari).
E-mail addresses: entezari@um.ac.ir (M.H. Entezari), moosavibaigi@um.ac.ir (F. Moosavi).

phenomena for changing SFE of solid surface is fabrication of superhydrophobic (SH) surfaces. SH surfaces possess water contact angle (CA) higher than 150° and can be classified into two categories based on sliding angle (SA) values which are low adhesive (with SA lower than 10°) and high adhesive (with very high SA) SH surfaces [2]. In other words, for rough surfaces, the Wenzel [3] and Cassie-Baxter [4] models can be applied to describe wetting state. In Wenzel model, a water droplet is able to enter to the asperities and totally fill any surface groove. The factor of roughness in Wenzel equation can improve the innate state of the material and gives a lower CA to hydrophilic surfaces and a larger CA to hydrophobic ones. The Cassie-Baxter model establishes another novel wetting state, in which air molecules may be trapped in the asperities and the air-water interface allows free movement of droplet which induces low SA. Though both of these wetting models (Cassie-Baxter and Wenzel) cause high CA, just only the Cassie-Baxter state results in very low SA. Therefore, a true low adhesive SH surface considerably matches to the Cassie-Baxter state [5]. As a result, CA measurement on the surfaces is not sufficient for surface wettability description and it is essential to report SA accompanied with CA.

To create SH surfaces, it is essential to perform roughness improvement as a first step and SFE reduction as the second one [6–10]. In other words, as well the chemicals with low surface energy, the formation of multiple scales structures on material surfaces is a crucial necessity for superhydrophobicity [11].

A variety of techniques has been developed for roughness production. For example, sol-gel method, phase separation, solution immersion method, plasma etching, lithographic, and electrochemical deposition are practical ways for this purpose [12–20]. Furthermore, costly silanes or fluorides were applied for SFE reduction in the final step of SH surface processing. It is well identified that treatment with fluoride can efficiently diminish the SFE. However, flour derivatives are not essential materials to generate SH surfaces and there are alternatives for these materials [21].

In comparison with conventional surfactants, stearic acid (STA) is a good choice in superhydrophobicity field due to its low cost, biocompatibility, and low toxicity [22,23]. STA has low surface energy and its grafting on rough surface results in superhydrophobicity property. There are many works relating to SH surfaces. In these works, the SFE reduction after superhydrophobicity creation has been assessed qualitatively [24–26]. In the current study, our goal is to present a quantitative estimation of SFE reduction after superhydrophobicity. Therefore, it is necessary to compute SFE of Al metal at room temperature and then SFE calculation of SH Al to conclude that how much SFE changes.

SH Al surface possesses a low SFE value; as a result, equation of state and critical surface tension approaches are applicable to achieve SFE value for this surface. These methods (equation of state and critical surface tension) as appealing findings have been introduced for surfaces with insignificant SFE values (such as polymers [27]).

From the other side of view, Al enjoys a high SFE, i.e. equation of state and critical surface tension methods are not applicable for this condition. Therefore, it is necessary to employ another method to examine SFE. One accurate method is liquid surface tension measurement, which is carried out precisely [1]. Interestingly, the surface tension of molten metal can be determined experimentally and computed theoretically. The experimental routes are drop weight (DW), sessile drop (SD), etc. that are accomplished in the gaseous environment [28]. The inconsiderable amount of impurities in the gas plays a key role in the accuracy of measurement. Consequently, reports on the surface tension values witness the diversity of quantities as Keene claims [29]. In other words, because of melt contamination and high reactivity, exact values of surface tension are difficult to be acquired via straight experimental techniques. In these conditions, computational and theoretical methods are present as practical means to evaluate the surface tension accurately [28]. One of the computation methods to evaluate surface tension of liquid metals is computer simulation [30,31] in addition to the various theories in statistical mechanics [32–35] and density functional theory [36]. If the liquid metal surface tension is computed accurately, it is possible to correlate it with SFE of solid metal at the melting point. For instance, Tyson and Miller [1] have introduced a correlation between SFE of solid metal at the melting point with this property at different temperatures. By applying SFE of solid metal at the melting point, it is possible to compute SFE values of solid metal at ambient temperature according to Eq. (1).

$$\gamma_{sv} - \gamma_{sv}(T_m) = \int_T^{T_m} \frac{S_{sv}}{A} dT \qquad (1)$$

where γ_{sv} and $\gamma_{sv}(T_m)$ are SFE of solid Al at T and T_m, respectively, S_{sv} is surface entropy, and A is introduced as surface area per mole of surface atoms.

Recently, Rezayi and Entezari [37] have synthesized SH Al surface using ultrasound as a novel technique. In the present study, one goal is to examine SFE value change due to superhydrophobicity creation. In spite of several papers about surface tension calculation of liquid metals and SFE measurement of various solids [38–41], the number of publications on SFE comparison before and after superhydrophobicity processing is scarce. Therefore, the main novelty of current investigation is the mentioned issue. Based on experimental results (water CA measurement and ATR-FTIR analysis) [37], SFE of Al decreases considerably after SH creation which is in acceptable agreement with the current results. Another purpose is to verify this observation theoretically. In the present study, surface tension of liquid Al at melting point is computed by MD simulation. Afterward, SFE of solid Al at melting point was obtained using their correlation. To obtain SFE of Al at ambient temperature, a suitable equation was taken into consideration (Eq. (1)). Eventually, for SH Al, equation of state and critical surface tension approaches were used to measure SFE. The comparison between SFE results before and after superhydrophobicity process demonstrated the SFE reduction quantitatively. For SH Al, SFE is nearly equal to STA surface tension. Besides, experimental data confirm the presence of STA after modification that computational results are in excellent agreement with experiment.

2. Methods: theory and experiment

2.1. SFE calculation

Based on EDX results [37], Al plate is actually an alloy containing 96% Al and 4% Mg; consequently, considering Mg atoms in Al structure is an essential part of the study. In the present MD simulation study, NVT ensemble containing 256 atoms (241 Al atoms and 15 Mg atoms) in an orthorhombic cell with dimensions of $16.16 \times 16.16 \times 40.80 \text{ Å}^3$ was applied. Berendsen thermostat has been utilized in order to control the temperature with a relaxation time of 1.00 ps. Furthermore, Gupta potential was selected for the interatomic interaction of Al-Al, Mg-Mg, and Al-Mg particles in the system [42,43]. The simulations were carried out at a temperature range from T = 900 K to T = 1100 K at ambient pressure. The time step was 1.00 fs and all simulations were continued up to 5 ns, performed by DL_POLY_2.17 [44,45]. Solid Al SFE at desirable temperatures is followed by Eq. (1) [1] where S_{sv} can be written as the sum of configurational and vibrational contributions:

$$S = S_{sv}^{conf} + S_{sv}^{vib} \qquad (2)$$

The vibrational involvement is derived from reformed vibrational modes of surface atoms in comparison with internal atoms. It is predictable that these modes, similar to the bulk modes, will be gradually excited with temperature increase. Therefore, S_{sv}^{vib} is a time-dependent variable which has been assessed by Tyson and Miller [1]. As they have stated, a linear relation is observed for dependency between S_{sv}^{vib} and temperature ranging from zero at 0 K to $0.8R$ at $T/T_m = 0.2$ while at temperatures between $0.2T_m$ and melting point S_{sv}^{vib} remains constant at $0.8R$ [1]. Moreover, the configurational entropy must vary from a value close to zero at $T/T_m = 0.5$ to almost universal gas constant, R, at T_m [1].

According to Eq. (1), calculating γ_{sv} at melting temperature is a crucial step to be able to estimate solid SFE at various temperatures. This purpose is established by computing surface tension of the liquid (γ in J/m^2) that is calculated as [46]:

$$\gamma = -b_z \frac{(P_{xx} + P_{yy} - 2P_{zz})}{4} \qquad (3)$$

where b_z is the length of the simulation box along the z-axis. P_{xx}, P_{yy}, and P_{zz} are the main components of pressure tensor obtained from MD simulation at each temperature. When surface tension of molten Al is calculated, SFE of solid at melting temperature can be estimated based on the following relation [1]:

$$\gamma_{sv} = 1.18\gamma_{lv} \qquad (4)$$

which is valid for metals at the melting point. Having γ_{sv} at melting temperature, it is possible to evaluate solid Al SFE at any arbitrary temperature by the aid of Eq. (1). For SH Al surface, CA should be known in order to obtain SFE. Young equation is applied to obtain the value of CA, θ, [47]:

$$\gamma_{lv} \cos \theta = \gamma_{sv} - \gamma_{sl} \qquad (5)$$

where γ_{lv}, γ_{sv}, and γ_{sl} are liquid-vapor surface tension, solid-vapor surface tension (solid SFE), and solid-liquid interfacial tension, respectively. According to Eq. (5), calculating Young CA depends on accurate values of γ_{lv}, γ_{sv}, and γ_{sl} though only γ_{lv} and θ are measurable. As a result, an extra relation is necessary to obtain γ_{sv} and γ_{sl}. Numerous attempts have been made to overcome this issue. Initially, it has been represented [47] that γ_{sl} is a function of γ_{lv} and γ_{sv} as:

$$\gamma_{sl} = F(\gamma_{lv}, \gamma_{sv}) \qquad (6)$$

This relation is known as "equation of state for interfacial tension" [47] and is formulated as

$$\gamma_{sl} = \gamma_{lv} + \gamma_{sv} - 2\sqrt{\gamma_{lv} \cdot \gamma_{sv}} e^{-\beta(\gamma_{lv} - \gamma_{sv})^2} \qquad (7)$$

where β is a constant with a middling value of 0.0001247 (mJ/m^2)$^{-2}$.

Combining Young equation, Eq. (5), and interfacial tension equation of state, Eq. (7), Young CA is illustrated as

$$\cos \theta = -1 + 2\sqrt{\frac{\gamma_{sv}}{\gamma_{lv}}} e^{-\beta(\gamma_{lv} - \gamma_{sv})^2} \qquad (8)$$

It has been claimed previously [47] that solid SFE can be obtained by Eq. (8). In addition to equation of state method (Eq. (8)), another route has been employed to calculate SFE of SH Al named as critical surface tension [27] represented by attractive achievement for application of Young equation to find out γ_{sv} in the case of a solid with low surface free energy. In this procedure, the dependence of $\cos \theta$ on γ_{lv} is explored experimentally for a variety of liquids on a similar solid surface and a γ_{lv} value which is equivalent to $\cos \theta = 1$ extrapolated to achieve γ_{sv} value.

2.2. Experimental methods

2.2.1. Fabrication of SH Al

Based on our previous study [31], fabrication of SH Al was carried out. Briefly, at beginning, Al plates were polished carefully and washed with ethanol and distilled water to take away any contaminant. Then, cleaned Al substrates were placed into 50 ml aqueous solution of thriethylamine (TEA) (0.1 M) and Zinc acetate (Zn(AC)$_2$) (0.01 M) at 40 °C accompany with ultrasound injection for 15 min and with an amplitude of 40%. After withdrawing from the solution, Al plates were washed with distilled water and dried at 100 °C for 1 h. The as-synthesized ZnO-deposited Al substrate was modified using STA ethanol solution (0.021 M) for 1 h. Finally, Al substrates were washed with ethanol and dried at 80 °C for 10 min after withdrawing from STA ethanol solution. At this step, Al surface with water CA of 163.78° and SA about 2.33° were obtained, which possessed low adhesive SH state as well as being in Cassie-Baxter wetting situation. This surface was called as SH Al surface.

2.2.2. Fabrication of STA-modified Al

The first step was polishing and washing Al plates as mentioned above. At the second step, Al substrate was immersed in STA ethanol solution (0.021 M) for 1 h. Lastly, Al substrates were washed with ethanol after moving back from STA solution and dried at 80 °C for 10 min. This step resulted in STA-modified Al surfaces. The STA-modified Al has water CA of 93.75° with a hydrophobic property.

2.2.3. Characterization

An attenuated total reflection in conjunction with Fourier transform infrared spectrophotometry (ATR-FTIR, Shimadzu- IR- 460 spectrometer) was employed for chemical composition illustration of samples. ATR is nowadays the most commonly used FTIR sampling instrument. ATR, in general, allows sample analyzing with little or no sample preparation that significantly speeds sample examination. The main part of this instrument is a crystal which is in direct contact with sample [48]. The crystal employed for ATR analysis is ZnSe. Besides, the wavenumber range was 400–3000 cm^{-1} and the number of scans was 128. For assessment of surface morphology, a convenient technique is scanning electron microscopy (SEM). The SEM equipment with LEO 1450 VP and Germany model was applied.

There are several methods to explore CA value; some of them are captive bubble method [49], tilting plate method [50], Wilhelmy balance method [51], sessile drop method [52], and so on. Captive bubble method needs a large amount of liquid in addition to the being difficult if the solid swells after immersion into the liquid [53]. For tilting plate method, the major difficulty is a requirement of significant skills for CA identification [54]. On the other hand, Wilhelmy balance method suffers from several disadvantages which limit its usage. Indeed, the most commonly used technique for measuring CA is sessile drop method. This direct optical method benefits from its straightforwardness, an inconsiderable quantity of liquid required, and a small amount of surface substrate needed [55]. Considering these advantages, we applied the method to measure CA. The instrument employed here is a homemade one with important superiorities, such as simplicity and cost-effectiveness. A microsyringe was utilized for dropping off 10 microliter liquid droplets onto the surface of substrates. The images of droplets were captured using a camera (Canon SX200, Japan). Finally, the images were analyzed using MATLAB software to acquire CA. An inexpensive, useful, and uncomplicated apparatus was designed for SA measurements. This instrument has a movable plane. Al substrates were placed on this plane and water

droplet was placed on Al surface. Then, the plane was tilted until water droplet started to roll off.

3. Results and discussion

3.1. SFE of bare Al substrate

To achieve the results of the theoretical part, a series of MD simulations was carried out in order to compute surface tension of Al at melting temperature. To confirm the method and force field, the surface tension of molten Al at a number of temperatures above melting temperature was calculated. The variation of surface tension at ambient pressure with temperature, for the case under consideration, is shown in Fig. 1. As the figure illustrates, elevating temperature decreases the surface tension of molten Al. Certainly, this behavior is in accordance with experiment and demonstrates the temperature dependence of surface tension. Consequently, this trend supports the validity of force field applied. In addition, the experimental value for the surface tension of molten Al (96% Al - 4% Mg) at 973 K has been reported to be equal to 1031 mJ/m^2 [56]. This value is close to the theoretical one at this temperature (1056 mJ/m^2) and can be another witness for the validity of applied computational procedure.

One of our objectives is to evaluate γ_{sv} of bare Al at ambient temperature (298 K) to compare γ_{sv} values of bare and SH Al substrate. This goal is achievable if the combination of MD simulation with Eqs. (1) and (4) is performed. γ_{sv} at melting (920 K [57]) and ambient temperatures are summarized in Table 1. As Table 1 displays, by increasing the temperature from ambient to melting, the value of γ_{sv} observes a very slight decrease that is in accordance with solid interfacial behavior.

3.2. SFE of SH Al substrate

Based on water CA value results, water CA on bare Al is 45.00° that for SH Al increases significantly to 163.78°. Noticeably, it is obvious that SH Al substrate has low SFE; from the other point of view, we can apply equation of state and critical surface tension approaches to determine SFE. To obtain SFE of SH Al, based on Eq. (7), CA values of different liquids on target solid surface should be available. Here different liquids including polar and non-polar were employed; the values of relative polarity and surface tension are given in Table 2. Additionally, CA values of these liquids on SH Al surface and corresponding values of γ_{sv} are listed.

Based on two last columns of Table 2, the identity of applied liquid has a dramatic effect on CA values as well as γ_{sv} of SH Al.
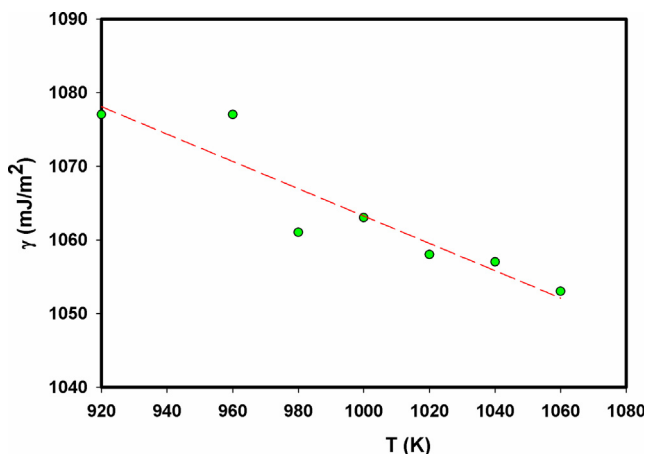
Fig. 1. Variation of surface tension of molten Al with temperature.

Table 1
γ_{sv} values for solid Al substrate at melting and ambient temperatures.

γ_{sv} (mJ/m^2)	T (K)
1271	920
1306	298

Generally, liquids with higher polarity lead CA raise; as a result, different values of γ_{sv} of SH Al changed vise verse. It means that different liquid characteristics play a role on γ_{sv} which also has been beforehand reported by Hejda et al. [58]. Moreover, it has been accomplished previously that some requirements such as surface smoothness are necessary to apply equation of state route [37]. Nonetheless, it is obvious that because of ZnO nanoparticle deposition during SH processing, the surface roughness improves and the smoothness necessity is not seen. Therefore, different values of γ_{sv} SH Al by various liquids were obtained. The roughness improvement after ZnO nanoparticle deposition can be proved based on SEM images. According to Fig. 2, bare Al has a roughly smooth surface (Fig. 2A). After deposition, the presence of numerous micro and nanostructures on Al surface was proved (Fig. 2B). This deposition was a major cause of roughness improvement. As a conclusion, the validity of roughness increment is a significant reason to observe deviation in γ_{sv} results using the equation of state route.

In order to eliminate surface roughness and verify the validity of equation of state as surface smoothness increases, equation of state method on polished Al surface after STA modification was repeated. After that, SFE of STA-modified with various liquid droplets was obtained, summarized in Table 3. It should be stated that the average value for SFE of STA-modified Al surface is 32.08 mJ/m^2.

In this case, in comparison with SH Al surface, Table 2, the variation of liquid type does not play any significant role on SFE value. In other words, because of surface smoothness, equation of state method is acceptable for STA-modified Al surface and the precision of results is acceptable. Additionally, it was demonstrated that for CA values in each case study, the plot of $\gamma_{lv} \cos \theta$ against γ_{lv} provided a smooth curve representing γ_{sv} as mentioned by Tavana et al. [59]. Figs. 3 and 4 illustrate the variation of $\gamma_{lv} \cos \theta$ versus γ_{lv} for SH Al and STA-modified Al, respectively. If CA deviates with respect to the curve, an uncertainty for exploring γ_{sv} will be introduced. In fact, the deviation is more obvious in the case of SH Al in comparison with STA-modified Al. On the other hand, CA values did not perfectly follow the curve in the case of SH Al; as a result, this observed scatter confirmed that equation of state method did not achieve an accurate value of γ_{sv}. Because of surface smoothness for STA-modified Al, all CA values approximately followed the curve; therefore, the conclusion drawn is that equation of state route is an appropriate method for similar cases.

Accurate insight to the figures shed light on insignificant deviation for non-polar and low-polar liquids that validates the accuracy for determining γ_{sv}. Fig. 5 illustrates this statement. According to this figure, the average γ_{sv} for the above-mentioned liquids was calculated to be equal to 26.60 mJ/m^2. Another result is that a superhydrophobe surface possessed a greater value of CA, especially bare Al surface enjoyed a water CA of 45.00° while SH Al observed that CA reaches to 163.78°. This noteworthy increase leads a significant decrease in SFE of Al substrate. The main reason for this reduction is STA grafting, at the second step of SH processing. ATR-AFTIR spectra corresponding to bare Al and SH Al are displayed in Fig. 6. According to the figure, the presence of long chain hydrocarbon and RCOO⁻ group were verified on SH Al. Since these groups are structural characteristics of STA [60], it was concluded that STA is grafted on SH Al during SH process.

Table 2
Properties of employed liquids including surface tension at ambient temperature and relative polarity as well as their CA results on SH Al surface and γ_{sv} values of SH Al.

Liquid	γ (mJ/m^2)	Relative polarity	CA (degree)	γ_{sv} (mJ/m^2)
Decalin	32.00	–	25.00	29.00
Tetralin	36.15	–	49.24	25.80
Pyridine	38.00	0.302	63.63	25.00
Benzyl alcohol	39.00	0.608	85.00	13.50
Dimethyl sulfoxide	43.54	0.444	122.00	3.60
Ethylene glycol	47.30	0.790	144.59	0.69
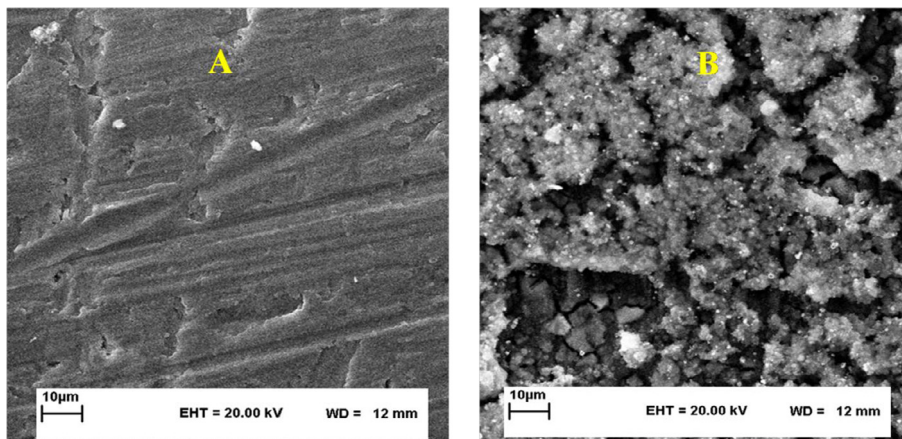
Fig. 2. SEM images of A) bare Al and B) ZnO- deposited Al.

Table 3
The calculated SFE (γ_{sv}) value of STA-modified Al by employing different liquids.

Liquid	CA (degree)	γ_{sv} (mJ/m^2)
Ethylene glycol	62.88	27.20
Dimethyl sulfoxide	42.42	29.90
Benzyl alcohol	29.26	32.60
Methyl salicylate	27.21	34.20
Pyridine	24.76	34.00
Tetralin	10.50	34.60

Fig. 4. $\gamma_{lv} \cos \theta$ versus γ_{lv} for studied liquids on STA- modified Al.
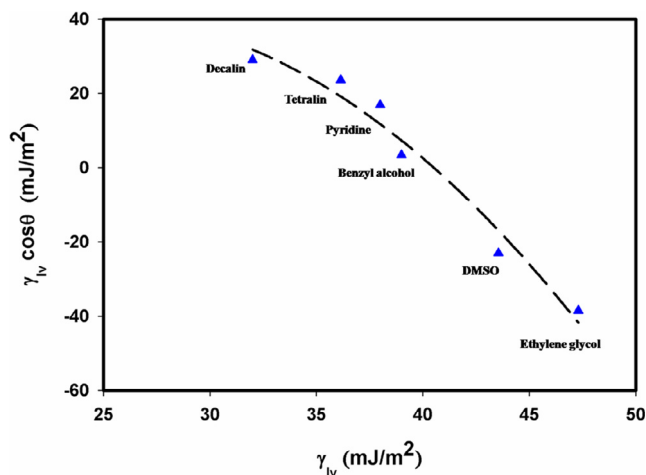

Fig. 3. $\gamma_{lv} \cos \theta$ versus γ_{lv} for studied liquids on SH Al.

Phankosol et al. [61] have reported that STA surface tension is 30.03 mJ/m^2 at ambient conditions. Logically, it was anticipated that such variation should be theoretically observed in Al SFE. Based on equation of state ro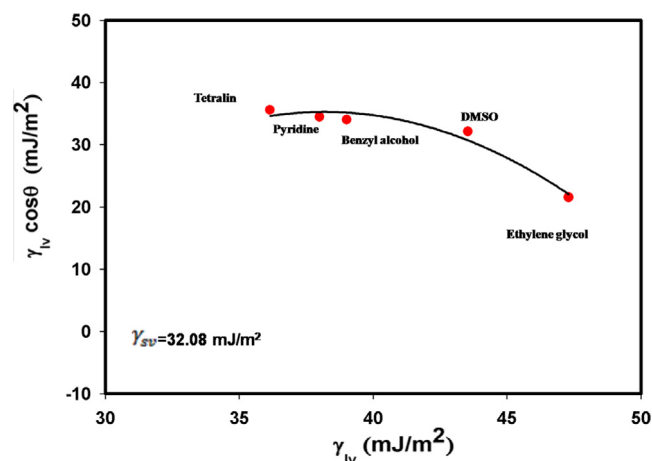ute, the computed SFE for SH Al is estimated to be 26.60 mJ/m^2 that is nearly close to the surface tension of STA. Interestingly, computational results accompany with experimental ones confirmed the existence of STA on SH Al.

However, in spite that equation of state route depends on liquid identity and its applicability for a smooth surface, it is more appropriate to evaluate SFE for estimation of STA-modified Al (Table 3 and Fig. 4). As our purpose was a determination of SFE of SH Al, it is recommended to calculate Al SFE by finding another method which is critical surface tension. At this state, CA quantity of various liquids (polar and non-polar) was measured on SH Al surface and the variation of $\cos \theta$ versus γ_{lv} was under consideration that is represented in Fig. 7. Now, SFE of SH Al is estimated by extrapolation of this curve to $\cos \theta = 1$ to find γ_{lv} as SFE of SH Al. According to this figure, SFE for SH Al is estimated to be 31.60 mJ/m^2. Besides, Fig. 7 indicates an acceptable linear trend by using various
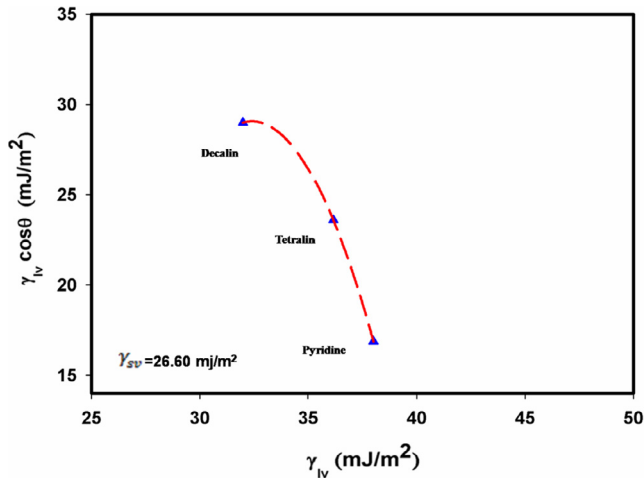
Fig. 5. $\gamma_{lv} \cos \theta$ versus γ_{lv} for studied non-polar and low polarity liquids on SH Al.
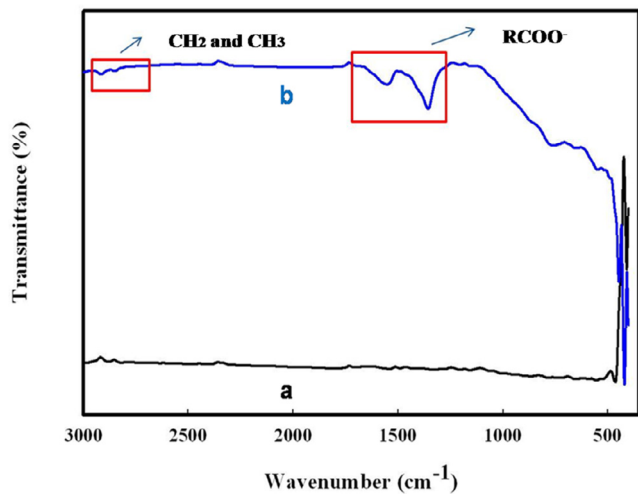

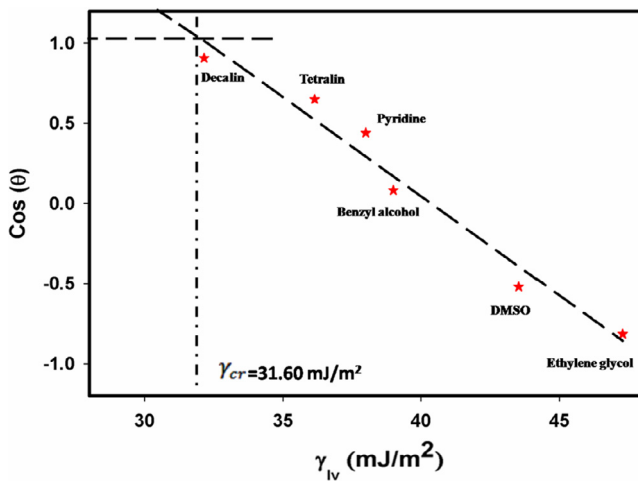**Fig. 6.** ATR-FTIR spectra for a) bare Al and b) SH Al.

Fig. 7. Zisman plot for SH Al surface with different liquids.

dissimilar liquids with different polarities. It can be stated that critical surface tension method is independent of liquid polarity, i.e. it is applicable for liquids with a wide range of characteristics. This

observation is in line with Rulison [62] study that surface roughness does not have any influence on critical surface tension validity and the linear trend is observed for different liquids that is a very admired evidence to apply this method.

4. Conclusion

The accurate accordance between SFE of STA (30.03 mJ/m^2) and SH Al (31.6 mJ/m^2) proves that critical surface tension is a more appropriate and accurate method to estimate SFE of SH Al. The observation of linear behavior with diverse liquids and validity of this method for rough surface verify the results. An important point is that selecting various methods for SFE calculation is based on the identity of studied surface. SFE of bare Al from MD at ambient temperature was 1306 mJ/m^2 that shows bare Al possesses a high surface energy. The reliability of MD simulation was verified via surface tension calculation of molten Al at different temperatures above the melting point. Besides, the comparison with experimental data and their agreement with each other is another reason for MD simulation reliability.

After creation of SH property, the SFE value was determined via equation of state and critical surface tension methods. Because of low SFE for SH Al, it is possible to apply equation of state technique, a simple semi-empirical route. The accuracy of this method is significantly influenced by CA values. Therefore, CA measurement for this technique is a crucial step. For this reason, CA was measured three times and the average values were reported. However, since this method depends considerably on the surface roughness, the required data were distributed over a wide range. As a result, critical surface tension approach that is independent of surface roughness and identity of employed liquids was utilized. The acceptable agreement between obtained results was taken as a sign of method consistency and demonstrated the precision of the method.

From the other side of view, CA measurement demonstrates SH Al possesses a greater CA value than bare Al which represents SFE reduction due to superhydrophobicity. The SFE of SH Al is equal to 31.60 mJ/m^2 based on critical surface tension route. As a result, the computational outcomes reveal SFE reduction after SH creation. In addition, ATR-FTIR spectra of SH Al confirm the presence of STA after surface modification. STA is a fatty acid with low surface energy and its grafting on SH Al is the main reason for SFE reduction. The theoretical calculated SFE for SH Al is close to the surface tension of STA. Overall, the experimental results (CA measurements and ATR-FTIR analysis) seeks to ascertain precisely the existence of STA on SH Al and surface energy reduction that are in agreement with theoretical results.

Acknowledgment

References

[1] W. Tyson, W. Miller, Surface free energies of solid metals: estimation from liquid surface tension measurements, Surf. Sci. 62 (1977) 267–276.
[2] J. Song, Y. Lu, S. Huang, X. Liu, L. Wu, W. Xu, A simple immersion approach for fabricating superhydrophobic Mg alloy surfaces, Appl. Surf. Sci. 266 (2013) 445–450.
[3] R.N. Wenzel, Resistance of solid surfaces to wetting by water, Ind. Eng. Chem. 28 (1936) 988–994.
[4] A. Cassie, S. Baxter, Wettability of porous surfaces, Trans. Faraday Soc. 40 (1944) 546–551.
[5] A.M. Escobar, N. Llorca-Isern, Superhydrophobic coating deposited directly on aluminum, Appl. Surf. Sci. 305 (2014) 774–782.
[6] J. Li, X. Liu, Y. Ye, H. Zhou, J. Chen, Fabrication of superhydrophobic CuO surfaces with tunable water adhesion, J. Phys. Chem. C 115 (2011) 4726–4729.

[7] R. Blossey, Self-cleaning surfaces—virtual realities, Nat. Mater. 2 (2003) 301–306.

[8] R. David, A.W. Neumann, Computation of the wetting properties of randomly structured superhydrophobic surfaces, J. Phys. Chem. C 116 (2012) 16601–16608.

[9] X. Gao, L. Jiang, Biophysics: water-repellent legs of water striders, Nature 432 (2004), 36-36.

[10] Z. She, Q. Li, Z. Wang, L. Li, F. Chen, J. Zhou, Novel method for controllable fabrication of a superhydrophobic CuO surface on AZ91D magnesium alloy, ACS Appl. Mater. Interfaces 4 (2012) 4348–4356.

[11] C.-L. Xu, F. Song, X.-L. Wang, Y.-Z. Wang, Surface modification with hierarchical CuO arrays toward a flexible, durable superhydrophobic and self-cleaning material, Chem. Eng. J. (2016).

[12] H. Budunoglu, A. Yildirim, M.O. Guler, M. Bayindir, Highly transparent, flexible, and thermally stable superhydrophobic ORMOSIL aerogel thin films, ACS Appl. Mater. Interfaces 3 (2011) 539–545.

[13] X. Feng, L. Feng, M. Jin, J. Zhai, L. Jiang, D. Zhu, Reversible super-hydrophobicity to super-hydrophilicity transition of aligned ZnO nanorod films, J. Am. Chem. Soc. 126 (2004) 62–63.

[14] N. Zhao, Q. Xie, L. Weng, S. Wang, X. Zhang, J. Xu, Superhydrophobic surface from vapor-induced phase separation of copolymer micellar solution, Macromolecules 38 (2005) 8996–8999.

[15] Y. Cui, A.T. Paxson, K.M. Smyth, K.K. Varanasi, Hierarchical polymeric textures via solvent-induced phase transformation: a single-step production of large-area superhydrophobic surfaces, Colloids Surf. A 394 (2012) 8–13.

[16] T. Ishizaki, N. Saito, Rapid formation of a superhydrophobic surface on a magnesium alloy coated with a cerium oxide film by a simple immersion process at room temperature and its chemical stability, Langmuir 26 (2010) 9749–9755.

[17] W. Xu, H. Liu, S. Lu, J. Xi, Y. Wang, Fabrication of superhydrophobic surfaces with hierarchical structure through a solution-immersion process on copper and galvanized iron substrates, Langmuir 24 (2008) 10895–10900.

[18] J. Park, H. Lim, W. Kim, J.S. Ko, Design and fabrication of a superhydrophobic glass surface with micro-network of nanopillars, J. Colloid Interface Sci. 360 (2011) 272–279.

[19] K. Teshima, H. Sugimura, Y. Inoue, O. Takai, A. Takano, Transparent ultra water-repellent poly (ethylene terephthalate) substrates fabricated by oxygen plasma treatment and subsequent hydrophobic coating, Appl. Surf. Sci. 244 (2005) 619–622.

[20] E.-C. Cho, C.-W. Chang-Jian, H.-C. Chen, K.-S. Chuang, J.-H. Zheng, Y.-S. Hsiao, K.-C. Lee, J.-H. Huang, Robust multifunctional superhydrophobic coatings with enhanced water/oil separation, self-cleaning, anti-corrosion, and anti-biological adhesion, Chem. Eng. J. 314 (2016) 347–357.

[21] W. Zhang, P. Lu, L. Qian, H. Xiao, Fabrication of superhydrophobic paper surface via wax mixture coating, Chem. Eng. J. 250 (2014) 431–436.

[22] T. Wu, Y. Pan, L. Li, Study on superhydrophobic hybrids fabricated from multiwalled carbon nanotubes and stearic acid, J. Colloid Interface Sci. 348 (2010) 265–270.

[23] S. Theneshkumar, D. Gnanaprakash, N. Nagendra Gandhi, Solubility and mass transfer coefficient enhancement of stearic acid through hydrotropy, J. Chem. Eng. Data 55 (2010) 2980–2984.

[24] W. Liu, Y. Luo, L. Sun, R. Wu, H. Jiang, Y. Liu, Fabrication of the superhydrophobic surface on aluminum alloy by anodizing and polymeric coating, Appl. Surf. Sci. 264 (2013) 872–878.

[25] Y. Guo, Q. Wang, T. Wang, Facile fabrication of superhydrophobic surface with micro/nanoscale binary structures on aluminum substrate, Appl. Surf. Sci. 257 (2011) 5831–5836.

[26] Z. Yuan, J. Bin, X. Wang, C. Peng, M. Wang, S. Xing, J. Xiao, J. Zeng, X. Xiao, X. Fu, Fabrication of superhydrophobic surface with hierarchical multi-scale structure on copper foil, Surf. Coat. Technol. 254 (2014) 151–156.

[27] A.I. Rusanov, V.A. Prokhorov, Interfacial Tensiometry, Elsevier, 1996.

[28] F. Aqra, A. Ayyad, Surface tension (γLV), surface energy (γSV) and crystal-melt interfacial energy (γSL) of metals, Curr. Appl. Phys. 12 (2012) 31–35.

[29] B. Keene, Review of data for the surface tension of pure metals, Int. Mater. Rev. 38 (1993) 157–192.

[30] M. González-Melchor, F. Bresme, J. Alejandre, Molecular dynamics simulations of the surface tension of ionic liquids, J. Chem. Phys. 122 (2005) 104710.

[31] T. Zykova-Timan, D. Ceresoli, U. Tartaglino, E. Tosatti, Why are alkali halide surfaces not wetted by their own melt?, Phys Rev. Lett. 94 (2005) 176105.

[32] I.W. Plesner, O. Platz, Statistical-mechanical calculation of surface properties of simple liquids and liquid mixtures. I. Pure liquids, J. Chem. Phys. 48 (1968) 5361–5364.

[33] I.W. Plesner, O. Platz, S. Christiansen, Statistical-mechanical calculation of surface properties of simple liquids and liquid mixtures. II. Mixtures, J. Chem. Phys. 48 (1968) 5364–5370.

[34] R. Fowler, A tentative statistical theory of Macleod's equation for surface tension, and the parachor, Proc. R. Soc. London, Ser. A (1937) 229–246.

[35] M. Amin, R. Gosh, G. Bhuiyan, Surface tension of liquid transition and noble metals, J. Non-Cryst. Solids 380 (2013) 42–47.

[36] Y. Martinez-Raton, E. Velasco, A. Somoza, L. Mederos, T. Sluckin, Theoretical study of the anomalous surface tension properties of liquid crystals, J. Chem. Phys. 108 (1998) 2583–2593.

[37] T. Rezayi, M.H. Entezari, Towards a durable superhydrophobic aluminum surface by etching and ZnO nanoparticle deposition, J. Colloid Interface Sci. (2015).

[38] X. Tang, J. Gross, Density functional theory for calculating surface tensions with a simple renormalization formalism for the critical point, J. Supercrit. Fluids 55 (2010) 735–742.

[39] M.J. Spencer, A. Hung, I.K. Snook, I. Yarovsky, Density functional theory study of the relaxation and energy of iron surfaces, Surf. Sci. 513 (2002) 389–398.

[40] F. Aqra, A. Ayyad, Surface energies of metals in both liquid and solid states, Appl. Surf. Sci. 257 (2011) 6372–6379.

[41] K. Wojciechowski, Surface energy of metals: theory and experiment, Surf. Sci. 437 (1999) 285–288.

[42] W. Zhang, F. Zhang, Z. Zhu, On the melting phase transition of aluminum clusters around 55 atoms, Eur. Phys. J. D 43 (2007) 97–100.

[43] X. Li, Y. Qin, J. Fu, Z. Zhao, A Gupta potential for magnesium in hcp phase, Comput. Mater. Sci. 98 (2015) 328–332.

[44] W. Smith, Guest Editorial: DL_POLY–applications to molecular simulation II, Mol. Simul. 32 (2006), 933-933.

[45] W. Smith, T.R. Forester, DL_POLY_2.0: a general-purpose parallel molecular dynamics simulation package, J. Mol. Graph. 14 (1996) 136–141.

[46] M.H. Ghatee, A.R. Zolghadr, F. Moosavi, Y. Ansari, Studies of structural, dynamical, and interfacial properties of 1-alkyl-3-methylimidazolium iodide ionic liquids by molecular dynamics simulation, J. Chem. Phys. 136 (2012) 124706.

[47] H. Tavana, F. Simon, K. Grundke, D. Kwok, M. Hair, A. Neumann, Interpretation of contact angle measurements on two different fluoropolymers for the determination of solid surface tension, J. Colloid Interface Sci. 291 (2005) 497–506.

[48] H.W. Siesler, Infrared and Raman Spectroscopic Imaging, John Wiley & Sons, 2009.

[49] W.M. Schoel, S. Schürch, J. Goerke, The captive bubble method for the evaluation of pulmonary surfactant: surface tension, area, and volume calculations, Biochim. Biophys. Acta (BBA) 1200 (1994) 281–290.

[50] N.K. Adam, G. Jessop, Chem. Soc (1925) 1863.

[51] L. Wilhelmy, Ueber die Abhängigkeit der Capillaritäts-Constanten des Alkohols von Substanz und Gestalt des benetzten festen Körpers, Ann. Phys. 195 (1863) 177–217.

[52] W. Bigelow, D. Pickett, W. Zisman, Oleophobic monolayers: I. Films adsorbed from solution in non-polar liquids, J. Colloid Sci. 1 (1946) 513–538.

[53] W. Zhang, M. Wahlgren, B. Sivik, Membrane characterization by the contact angle technique, Desalination 72 (1989) 263–273.

[54] A.L. Speece, C.P. Rutkowski, G.L. Gaines Jr., Apparatus for the measurement of small contact angles between liquids and solids, Rev. Sci. Instr. 28 (1957) 636–637.

[55] W.C. Bigelow, D.L. Pickett, W.A. Zisman, Oleophobic monolayers, J. Colloid Sci. 1 (1946) 513–538.

[56] C. Garcia-Cordovilla, E. Louis, A. Pamies, The surface tension of liquid pure aluminium and aluminium-magnesium alloy, J. Mater. Sci. 21 (1986) 2787–2792.

[57] H. Okamoto, Al-Mg (aluminum-magnesium), J. Phase Equilib. 19 (1998) 598.

[58] F. Hejda, P. Solar, J. Kousal, Surface free energy determination by contact angle measurements–a comparison of various approaches, WDS (2010) 25–30.

[59] H. Tavana, A. Neumann, Recent progress in the determination of solid surface tensions from contact angles, Adv. Colloid Interface Sci. 132 (2007) 1–32.

[60] S. Wang, J. Shi, C. Liu, C. Xie, C. Wang, Fabrication of a superhydrophobic surface on a wood substrate, Appl. Surf. Sci. 257 (2011) 9362–9365.

[61] S. Phankosol, K. Sudaprasert, S. Lilitchan, K. Aryusuk, K. Krisnangkura, Estimation of surface tension of fatty acid methyl ester and biodiesel at different temperatures, Fuel 126 (2014) 162–168.

[62] C. Rulison, So you want to measure surface energy, A tutorial designed to provide basic understanding of the concept solid surface energy, and its many complications, TN306/CR (1999) 1–16.